Epitope specificity determines pathogenicity and detectability of anti-platelet-derived growth factor receptor α autoantibodies in systemic sclerosis

Arthritis & Rheumatology
DOI 10.1002/art.39125

Epitope specificity determines pathogenicity and detectability of anti-PDGFRα autoantibodies in systemic sclerosis

Gianluca Moroncini[1,2]*, Antonella Grieco[1#], Giulia Nacci[3#], Chiara Paolini[1#], Cecilia Tonnini[1,2], Katarzyna N. Pozniak[1], Massimiliano Cuccioloni[4], Matteo Mozzicafreddo[4], Silvia Svegliati[1], Mauro Angeletti[4], Andrius Kazlauskas[5], Enrico V. Avvedimento[6], Ada Funaro[3], Armando Gabrielli[1,2]*.

[1]Dipartimento di Scienze Cliniche e Molecolari, Università Politecnica delle Marche, Ancona, 60126 Italy.

[2]Clinica Medica, Ospedali Riuniti Ancona, 60126 Italy.

[3]Dipartimento di Scienze Mediche, Università di Torino, 10126 Italy.

[4]Scuola di Bioscienze e Medicina Veterinaria, Università di Camerino, 62032 Italy.

[5]Schepens Eye Research Institute, Harvard Medical School, Boston, MA 02114 USA.

[6]Dipartimento di Medicina molecolare e Biotecnologie mediche, Università Federico II, Napoli, 80131 Italy.

# These authors contributed equally.

*To whom correspondence should be addressed: G.M. (g.moroncini@univpm.it) and A.G. (a.gabrielli@univpm.it).

Received: Jul 17, 2014; Revised: Feb 09, 2015; Accepted: Mar 17, 2015

Objective. This study aimed at cloning autoantibodies targeting the PDGF receptor α (PDGFRα) from B cells of one patient with Systemic Sclerosis (SSc), to identify the epitopes recognized by these autoantibodies and develop novel assays for detection of serum anti-PDGFRα autoantibodies.

Methods. EBV-immortalized B cells were screened for expression of IgG binding to PDGFRα and inducing reactive oxygen species (ROS) in fibroblasts. The variable (V) regions of anti-PDGFRα IgG were cloned into an IgG expression vector to generate distinct recombinant human monoclonal autoantibodies (rHumaab), which were characterized by binding and functional assays. The epitopes of anti-PDGFRα rHumaab were defined by molecular docking; surface plasmon resonance binding assays; screening of a conformational peptide library spanning the PDGFRα extracellular domains; expression of alanine-scanned PDGFRα mutants. Direct or competitive ELISAs were established to detect all the anti-PDGFRα antibodies or selectively the agonistic ones.

Results. Three types of anti-PDGFRα rHumaab, with the same VH but distinct VL chains, were generated. Non-agonistic VH_{PAM}-Vκ13B8 recognized one linear epitope, whereas agonistic VH_{PAM}-Vλ16F4 and VH_{PAM}-Vk16F4 recognized two distinct conformational epitopes. Serum anti-PDGFRα antibodies were detected in 66/70 SSc, 63/130 healthy controls (HC), 11/26 Primary Raynaud's Phenomenon (PRP) and 13/29 SLE patients. Serum VH_{PAM}-Vk16F4-like antibodies were found in 24/34 SSc, but not in HC, PRP or SLE. Peptides composing the VH_{PAM}-Vk16F4 epitope inhibited PDGFRα signaling triggered by SSc IgG.

Conclusion. Agonistic anti-PDGFRα autoantibodies are enriched in SSc sera and recognize specific conformational epitopes, that can be used to discriminate agonistic from nonagonistic antibodies and block PDGFRα signaling in SSc.

Systemic sclerosis or scleroderma (SSc) is a clinically heterogeneous disease of the connective tissue characterized by vascular, immune/inflammatory and fibrotic manifestations, in which oxidative stress is a prominent feature (1, 2). Despite extensive investigations, the key pathogenic links between these disease hallmarks remain obscure, which hampers the development of tools for early diagnosis, adequate disease monitoring and effective therapies. We have previously reported the presence of agonistic anti-Platelet Derived Growth Factor Receptor (PDGFR) autoantibodies stimulating reactive oxygen species (ROS) in the serum IgG of 46 SSc patients (3). However, other studies (4, 5) failed to detect these stimulatory antibodies in the serum, and found non-stimulatory anti-PDGFR antibodies both in SSc and healthy controls (HC) (5) or in patients with Systemic Lupus Erythematosus (SLE) (6). Hence, the presence of stimulatory anti-PDGFR autoantibodies in SSc remains controversial (7). To address this issue, we generated combinatorial monoclonal autoantibodies using immunoglobulin sequences identified in memory B cells of one SSc patient, specific for PDGFRα, the isoform which better discriminated SSc IgG from HC IgG (3). By these reagents, we obtained a novel map of the functional epitopes of PDGFRα selectively driving oxidative stress and increase of collagen gene expression. Moreover, we assessed the clinical relevance of this finding by developing novel binding assays for anti-PDGFRα autoantibodies.

Patients and Methods

Ethics statements

Use of human material was approved by the Institutional Ethical Committee of Università Politecnica delle Marche, Ancona, Italy, and consent was obtained from all subjects participating to this study. All assays were performed in blind fashion on coded samples.

Screening of immortalized memory B cells

CD22-positive memory B cells were purified by magnetic selection (Miltenyi Biotech) from peripheral blood mononuclear cells (PBMC) of one patient with diffuse SSc (8) with oesophagus and lung involvement (code: PAM, female, 47 years old, Rodnan skin score 17, ANA and anti-Scl 70 positive, anticentromere negative). Cells were immortalized using Epstein-Barr virus (EBV) as described (9-11). Three days post-infection, cells were manually counted and seeded (5 cells/well) in 96-well plates in the presence of irradiated (30 Gy) allogenic PBMC. After 2 weeks, B cell supernatants were screened for the presence of anti-PDGFRα antibodies by immunofluorescence and flow cytometry using mouse fibroblasts derived from PDGFR-knockout embryos (F-/-) transfected with full-length human PDGFRα (Fα) (12) as target cells, as described (3).

Generation of recombinant human monoclonal autoantibodies

Total RNA was extracted from each anti-PDGFRα positive B cell line (~300.000 cells) with RNeasy Micro Kit and reverse-transcribed with Omniscript RT Kit (Qiagen). cDNA was amplified with PCR primers specific for human rearranged IgG variable (V) and constant (C), heavy (H) and light (L) chain genes (13) (Supplementary Table 1). Amplified H and L chain V regions were sequenced by TOPO TA Cloning Kit (Invitrogen). The unique VH and the four different VL chain sequences amplified in three PAM B cell lines showing PDGFRα binding were alternatively paired to replace VH and VL chains of antibody b12 (14), generating four distinct human IgG_1 constructs. VH and VL sequences were fused with the respective leader peptide sequences using a three-step overlap extension PCR (15), then independently inserted into the XbaI-SacI and HindIII-EcoRI restriction sites of pDR12 vector containing the parental human IgG_1 constant chain genes, including the Fc sequence. Upon sequencing, the constructs were stably transfected into Chinese hamster ovary (CHO) cells with Lipofectamine 2000 (Invitrogen). Expression of recombinant IgG in culture supernatant was confirmed by human IgG-specific ELISA. Cell cultures were expanded

in bioreactors (CELLine CL-1000, Integra Biosciences) and secreted recombinant human monoclonal autoantibodies (rHumaab) were purified from supernatants by Protein A affinity and size exclusion chromatography. Purity of rHumaab was checked by SDS-PAGE Coomassie Brilliant Blue protein staining.

Immunoprecipitation and Immunoblotting

Each rHumaab (10 µg/ml) was incubated for 4 hours at 4°C with 100 µg of total protein extracts from human fibroblasts. The mixture was incubated overnight at 4°C with 20 µl of agarose-Protein A/G (Santa Cruz), and the immunocomplexes were subjected to SDS-PAGE and immunoblotting as described (3).

Functional assays

Primary human fibroblasts from adult healthy skin (HDF, Life Technologies) were cultured in DMEM with 10% FCS for two passages. At sub-confluence, cells were maintained in 0.2% FCS for 24 hours, before addition of human PDGF-BB (15 ng/ml), TGF-β (2 ng/ml) (R&D Systems) or rHumaab (10 µg/ml). Protein extracts (30 µg) were separated on 4-12% SDS-PAGE under reducing conditions and transferred to PVDF membranes. After blocking, membranes were probed with anti-pAKT (sc-439), anti-pERK (sc-7783), anti-Ha-Ras (sc-520), stripped and re-probed with anti-total AKT, ERK1/2 and β-actin (Santa Cruz Biotechnologies), followed by HRP-conjugated antibodies.

To quantify collagen gene transcription, total RNA was extracted (Aurum total RNA mini Kit, Bio-Rad) from fibroblasts at baseline and after 1 hour stimulation as indicated. The purity of RNA templates measured as 260/280 nm ratio (Nanodrop, Thermo Scientific) was in the 1.8-2.1 range. RNA (1 µg) was reverse transcribed with iScript cDNA synthesis Kit (Bio-Rad). Human Col1A1 and Col1A2 genes were measured by real-time PCR with iQ SYBR Green Supermix and iCycler (Bio-Rad). Primers: HuCol1A1 fw: 5'-AGGGCCAAGACGAAGACATC-3'; HuCol1A1 rev: 5'-

AGATCACGTCATCGCACAACA-3'; HuCol1A2 fw: 5'-AGGTCAAACAGGAGCCCGTGGG-3'; HuCol1A2 rev: 5'-GCACCTGGGAAGCCTGGAGGG-3'; HuGAPDH fw: 5'-TGCACCACCAACTGCTTAGC-3'; HuGAPDH rev: 5'-GGCATGGACTGTGGTCATGAG-3'; Hu18SrRNA fw: 5'-TCCCCATGAACGAGGAATTC-3'; Hu18SrRNA rev: 5'-GTGTACAAAGGGCAGGGACTT-3'. PCR conditions: 95°C for 3 minutes, then 95°C for 15 seconds, 58°C for 60 seconds (45 cycles).

The ROS bioassay (fluorimetric determination of intracellular ROS generated by adherent fibroblasts) was performed as described (16).

Homology modeling and molecular docking

Homology modeling to predict the unknown three-dimensional structures of human PDGFRα and rHumaab Fab monovalent fragments from their amino-acid sequences was performed using Swiss-Model server (17). Swiss-Pdb Viewer software was used to create project files submitted to the server with default parameters settings (BLAST search $P < 0.00001$ and global degree of sequence identity SIM > 25%). PDGFRα query sequences were obtained from UniProt Knowledgebase (http://beta.uniprot.org/). Rigid protein-protein molecular docking between homology-modeled monomeric PDGF-BB (pdb-ID: 1PDG) (18), rHumaab Fabs, and monomeric PDGFRα was performed uploading the pdb files on ClusPro 2.0 server (19) and setting DOT 1.0 as docking program, a clustering radius of 5Å, electrostatic hits of 1500 and 30 final resulting structures (data available upon request).

Generation and screening of PDGFRα peptide library

Eighty overlapping 15-oligomer synthetic peptides spanning the first three N-terminal, extracellular Ig-like domains of PDGFRα were flanked by either glycines or cysteines (Cys). Glycine-flanked peptides were left in linear conformation, whereas Cys-flanked peptides were imposed on a trivalent

(T3) chemical scaffold [containing three PhCH2Br (1,3,5-tribromomesitylene, T3) groups reacting 1:1 with the three Cys in the peptides, with the sequence: Cys-15-oligomer-Cys-15-oligomer-Cys] with spatially defined conformations to mimic a looped conformation. By virtue of this technology (Chemically LInked Peptides on Scaffolds, CLIPS, Pepscan Therapeutics BV) (20, 21), the eighty 15-oligomer segments were all combined with each other to obtain all the possible combinations of Cys-15-oligomer-Cys-15-oligomer-Cys bi-cyclical peptides (total T3-CLIPS 30-oligomer peptides = 6.400). The T3-CLIPS topology allows the peptides to have either a two looped folding or a loop plus partial sheet folding. The combinatory peptides were immobilized onto 455-well plates and binding of rHumaab and PDGF-BB was tested by PEPSCAN-based ELISA.

Soluble peptides

Three peptides were synthesized (Pepscan Therapeutics BV) and numbered from 1 to 3 following the amino acid sequence of human extracellular PDGFRα from the N- to the C-terminus. Peptide 1: ac-VIVEDDDSAIIPCRTTD-conh2; peptide 2: ac-VVPASYDSRQGFNGTFTVGPYICE-conh2; peptide 3: ac-CAARQATREVKEMKKVT-conh2. Scrambled peptide 2: ac-IASGCGTFTRVVFEQPNSPYYDGV-conh2. HPLC purity was > 95%.

In binding-competition experiments, VH_{PAM}-Vκ16F4 (10 μg/ml), (molar ratio peptide: rHumaab = 100:1) or a pool of IgG from six SSc patients or HC (200 μg/ml) were incubated in solution with single peptides for 1 hour at 37°C, then used to stimulate fibroblasts.

PDGFRα mutagenesis and expression of PDGFRα mutants in F-/-

Five different sets of Alanine mutations were introduced into the epitope of VH_{PAM}-Vκ16F4. The template for mutagenesis (GenScript) was the full-length human PDGFRα cDNA inserted into the retroviral vector p*LHDCX2* (22). The PDGFRα mutants were termed Ala-scans and numbered from the N- to the C-terminus (according to the corresponding peptides): Ala-scan1: ^{109}EDDD^{112} to

^{109}AAAA^{112}, Ala-scan2: ^{149}TFT^{151} to ^{149}AAA^{151}, Ala-scan3: ^{262}QATR^{265} to ^{262}AAAA^{265}. Two longer Ala-scans were generated combining Ala-scan1 and 2 (Ala-scan4) or Ala-scan1, 2 and 3 (Ala-scan5). The five Ala-scans were individually transfected into PA317 cells (ATCC) with Lipofectamine to produce retroviral virions (23). Virus-containing medium was collected, concentrated (25,000 *g*, 90 minutes, 4°C) and used to infect F-/- cells (12) grown in DMEM with 8 µg/ml polybrene (hexadimethrine bromide; Sigma-Aldrich) for 24 hours. Successfully infected cells were selected in histidine-free DMEM containing 5 mM histidinol (Sigma-Aldrich) (24). Mutated PDGFRα expression was assessed by FACS using VH_{PAM}-Vκ16F4 and mab 1264 antibodies.

Immunoenzymatic assays (ELISA)

A recombinant receptor fused to a poly-Histidine tag (PDGFRα-His) produced in-house (25) or commercial (amino acid Met 1-Glu 524, cod. 10556-H08H, Sino Biological Inc.) were immobilized [0.5 µg/ml in 100 µl of Hepes buffered saline (HBS), pH 7.2] onto 96-well Maxisorp ELISA plates (Nunc) overnight at 4°C. After 2 hours blocking at 37°C with 200 µl of HBS containing 0.2% polyvinylpyrrolidone (Sigma-Aldrich) and washing with HBS/0.05% Tween 20, serum (1:100 in HBS, 100 µl/well) was added overnight at 4°C. After extensive washing, HRP-conjugated anti-human IgG (1:10.000, 100 µl/well) (Jackson Immunoresearch) were added for 1 hour at 20°C. The reaction was developed with 100 µl of tetramethylbenzidine (TMB, BioFX) for 10 minutes at room temperature, then stopped with 50 µl of 0.5 M H_2SO_4. The optical density (O.D.) was measured at 450 nm. In the peptide-based ELISA, 20 µg/ml of each peptide were immobilized onto 96-well plates and probed with 0.7 µg/ml of the indicated rHumaab. In the competitive ELISA, serum (1:100), VH_{PAM}-Vκ16F4 (0.7 µg/ml) or PDGF-BB (15 ng/ml) were pre-incubated with 25 µg/ml of the indicated peptide (molar ratio peptide : PDGFRα = 50:1) for 1 hour at 37°C. Alternatively, serum (1:100) was incubated with immobilized PDGFRα-His overnight at 4°C, before adding biotinylated VH_{PAM}-Vκ16F4 (ChromaLink Biotin Protein Labeling Kit Solulink, VWR

International) (100 ng/ml) for 2 hours at 37°C, followed by HRP-conjugated streptavidin (1:5.000) (Bio-Rad) for 1 hour at room temperature.

Statistical Analysis

Data are presented as means ± SEM or ± SD, as indicated, and were analyzed with one-way non-parametric ANOVA analysis with Kruskal-Wallis and Dunn's multiple comparison tests (peptide binding, direct and competitive ELISA) or two-tailed unpaired t test [confidence intervals (CI) 95%] (functional, cell-based assays). Spearman's rank correlation coefficient for non-parametric data was calculated between the percentage of inhibition of VH_{PAM}-Vκ16F4 binding to PDGFRα-His after incubation with sera and the percentage of binding inhibition of sera to PDGFRα after pre-incubation with peptide 2. ROC curves were generated to determine the area under the curve (AUC) with its 95% CI. The optimal cut-off values were chosen according to the highest Youden index [sensitivity + (1 − specificity)], calculated using MedCalc12 software. GraphPad Prism 5 and MedCalc12 software were used for all the statistical analysis. $P < 0.05$ was considered statistically significant.

Results

Cloning of agonistic and nonagonistic anti-PDGFRα autoantibodies from memory B cells of one SSc patient

Immortalized memory B cells from one SSc patient (coded PAM) (9-11) were seeded in 96-well plates. Supernatants of ~2.000 wells were screened for expression of IgG selectively binding Fα but not F-/- fibroblasts (12), and inducing ROS. Three B cell cultures (namely, PAM13B8, PAM16F4 and PAM17H8) contained PDGFRα-binding IgG, of which PAM16F4 IgG induced ROS (Figure 1A). RNA was extracted from these B cells, reverse-transcribed and amplified with primers designed to analyze the human IgG gene repertoire (13). PCR analysis of rearranged IgG genes

suggested the presence of a panel of VH and VL chains representative of most IgG subgroups (Figure 1B). However, subsequent sequencing revealed that most of these PCR products were similar, although not identical, at oligonucleotide level (Supplementary Figure 1), both within each single B cell culture and among the three cell cultures, indicating oligoclonal restriction. Indeed, PAM13B8, PAM16F4 and PAM17H8 cells shared a single VH chain amino acid sequence, designated VH_{PAM}, and a VL chain, designated Vλ13B8. Moreover, PAM 13B8 and 17H8 shared a Vκ chain designated Vκ13B8, whereas the repertoire of PAM16F4 included two additional VL chains (designated Vκ16F4 and Vλ16F4) (Figure 1B). The VH_{PAM} cDNA and, alternatively, each of the four VL_{PAM} cDNAs were cloned into an expression vector containing the human IgG_1 constant region (15) and transfected into CHO cells to produce four rHumaab, designated VH_{PAM}-Vκ13B8, VH_{PAM}-Vλ13B8, VH_{PAM}-Vκ16F4 and VH_{PAM}-Vλ16F4. All rHumaab, except VH_{PAM}-Vλ13B8, immunoprecipitated PDGFRα from human fibroblast lysates (Figure 1C). VH_{PAM}-Vκ16F4 and VH_{PAM}-Vλ16F4, but not VH_{PAM}-Vκ13B8 and VH_{PAM}-Vλ13B8, induced ROS production and ERK1/2 and AKT phosphorylation *in vitro* (Figure 1D). VH_{PAM}-Vκ16F4, but not VH_{PAM}-Vλ16F4, also induced Ha-Ras and type I collagen gene expression (Figure 1D). These data show that PDGFRα binding and biological effects of these rHumaab can be dissociated, suggesting the presence of different PDGFRα epitopes mediating such functions.

Epitope mapping of human PDGFRα

To identify the PDGFRα epitopes of the rHumaab, we used *in silico* molecular docking, *i.e.* a computer simulation of molecular interactions, as a starting model to predict the binding regions between homology-modeled monomeric human PDGFRα and rHumaab Fab fragments or monomeric human PDGF-BB, the only PDGF isoform with resolved crystal structure. PDGF-BB was predicted to bind a discontinuous epitope encompassing four amino acid segments lying

between the second and third Ig-like extracellular domains of PDGFRα (Figure 2A, pink sequences), which is consistent with previous studies (26, 27). The agonistic rHumaab VH_{PAM}-Vκ16F4 was predicted to bind to a discontinuous epitope within the second and third PDGFRα extracellular domains, largely overlapping the PDGF-BB binding site (Figure 2B, blue sequences). Conversely, the predicted epitope of the non-agonistic rHumaab VH_{PAM}-Vκ13B8 encompassed a single linear amino acid sequence within the first PDGFRα extracellular domain (Figure 2C, yellow sequence). Part of this sequence was shared by the larger, discontinuous epitope of the agonistic rHumaab VH_{PAM}-Vλ16F4, which comprised additional amino acid stretches in the first and second PDGFRα domains (Figure 2D, green sequences). To experimentally validate these predictive data, we screened with PDGF-BB and the rHumaab a conformational PDGFRα peptide library synthesized by Pepscan (28, 29). This approach highlighted a remarkable correspondence between the predicted (*in silico*) and the actual (*in vitro*) PDGFRα epitopes bound by rHumaab and by PDGF-BB (Figure 2A-C, underlined sequences), except VH_{PAM}-Vλ16F4, which did not bind to any peptide, probably for incomplete representation of its conformational epitope in the library. Notably, the highest binding peaks of PDGF-BB and VH_{PAM}-Vκ16F4 occurred with looped peptides (data available upon request), corroborating the conformational nature of their PDGFRα epitopes.

To further validate the PDGFRα epitope mapping, binding-competition experiments were performed on a Surface Plasmon Resonance (SPR) device where the PDGFRα-His, immobilized and folded into a native-like conformation (25), was saturated with PDGF-BB or single rHumaab before adding each rHumaab. The resulting sensorgrams (Figure 2B-D, insets) showed that binding of VH_{PAM}-Vκ16F4 to PDGFRα was completely prevented by PDGF-BB (Figure $2B^{\#}$), but only partially prevented by VH_{PAM}-Vκ13B8 (Figure $2B^{\#\#}$), likely for steric hindrance. VH_{PAM}-Vλ16F4 slightly inhibited VH_{PAM}-Vκ16F4 binding (Figure $2B^{\#\#\#}$). These data confirm that VH_{PAM}-Vκ16F4 (inducing both ROS and type I collagen genes) recognizes an epitope overlapping the PDGF

binding site, but distinct from the epitopes of VH_{PAM}-Vκ13B8 (non-agonistic) and VH_{PAM}-Vλ16F4 (inducing ROS, but not type I collagen genes). Conversely, binding of VH_{PAM}-Vκ13B8 and VH_{PAM}-Vλ16F4 to PDGFRα was not significantly inhibited by PDGF-BB (Figure 2 $C^{\#}$, $D^{\#}$). Finally, VH_{PAM}-Vκ13B8 and VH_{PAM}-Vλ16F4 showed partial reciprocal binding inhibition (Figure 2 $C^{\#\#\#}$, $D^{\#\#}$), consistent with the minimal overlap between their epitopes. We conclude that there are three distinct PDGFRα epitopes recognized by these antibodies. One epitope, largely shared by PDGF-BB and by the ROS- and collagen-inducing VH_{PAM}-Vκ16F4, is conformational and discontinuous. The second epitope, bound by VH_{PAM}-Vλ16F4, inducing ROS but not collagen, is also conformational and discontinuous. The third epitope, bound by VH_{PAM}-Vκ13B8, is an apparently nonfunctional single peptide in the first extracellular domain of PDGFRα.

Specific PDGFRα peptides interfere with binding and functions of VH_{PAM}-Vκ16F4 rHumaab and IgG from SSc patients

The three peptides corresponding to the PDGFRα sequences (Figure 2B, underlined sequences) composing the discontinuous epitope of VH_{PAM}-Vκ16F4, bound VH_{PAM}-Vκ16F4, but not VH_{PAM}-Vκ13B8 or VH_{PAM}-Vλ13B8 (Figure 3A). Pre-incubation with any of these peptides significantly inhibited VH_{PAM}-Vκ16F4 binding to PDGFRα (Figure 3B) and VH_{PAM}-Vκ16F4-mediated collagen gene induction (Figure 3C). Peptide 2 was the most effective inhibitor under these experimental conditions, it also significantly reduced PDGF binding (Figure 3B) and collagen gene induction and ROS production triggered by SSc IgG (Figure 3D). Peptide 1, but not peptide 3, inhibited SSc IgG-induced ROS production (Figure 3D). The scrambled peptide 2 did not bind to VH_{PAM}-Vκ16F4, PDGF-BB or SSc IgG nor inhibited their agonistic effects (Figure 3A-D).

Mutagenesis of the discontinuous epitope of the agonistic rHumaab VH_{PAM}-Vκ16F4

A limited Alanine scanning mutagenesis of the essential motifs (Figures 2B, blue sequences, and 4A) composing the VH_{PAM}-Vκ16F4 epitope was performed. Binding to VH_{PAM}-Vκ16F4 was retained by Ala-scans 1, 2, 3 (Figure 4B); however, collagen gene stimulation by VH_{PAM}-Vκ16F4 was observed with Ala-scans 1 and 3, but it was completely impaired by Ala-scan 2. (Figure 4C). This result is consistent with the finding that peptide 2 is the most effective inhibitor of VH_{PAM}-Vκ16F4-induced collagen stimulation (Figure 3C) and indicates that the TFT amino acid motif is essential for collagen induction. Expression of Ala-scan 4, spanning motifs 1 and 2, or Ala-scan 5, spanning motifs 1, 2 and 3 (Figure 4A), impaired both VH_{PAM}-Vκ16F4 binding and collagen stimulation (Figure 4B,C). These results independently validate the PDGFRα epitope mapping, highlighting the minimal extracellular PDGFRα motif required for collagen gene stimulation.

Detection of anti-PDGFRα autoantibodies in the serum of SSc patients

Three independent assays were established:

A. Direct ELISA with PDGFRα-His immobilized onto 96-well plates:

sera from 70 consecutive patients with a definite diagnosis of SSc (8) (Supplementary Table 2), from 130 sex- and age-matched HC, and 26 consecutive patients with a definite diagnosis of primary Raynaud's phenomenon (PRP) (30), were tested. Based on the optimal cut-off value determined by ROC curve analysis of SSc and HC O.D. values, 94.3% of SSc (66/70), 48.5% of HC (63/130) and 42.3% of PRP (11/26) sera were positive ($P < 0.0001$ between SSc and other groups) (Figure 5A). Similar results were obtained using a commercial PDGFRα-His (data available upon request), ruling out any artificial binding of serum IgG to the PDGFRα-His produced in-house. No sera showed non-specific binding to uncoated plates (not shown).

B. Competitive ELISA between immobilized PDGFRα-His and peptides covering the VH_{PAM}-Vκ16F4 epitope :

to evaluate the presence of serum anti-PDGFRα IgG recognizing the same epitope of the agonistic rHumaab VH_{PAM}-Vκ16F4, SSc and HC (n = 34 each) and PRP (n = 18) sera, chosen according to homogeneous O.D. frequency distributions in assay *A.*, were incubated with peptide 2 (the most effective inhibitor of VH_{PAM}-Vκ16F4 and SSc IgG, Figure 3B-D) before binding to immobilized PDGFRα. Based on the ROC curve optimal cut-off value, pre-incubation with peptide 2 significantly inhibited PDGFRα binding of 70.6% (24/34) of SSc sera, 11.7% (4/34) of HC and none (0/18) of PRP sera ($P < 0.001$ and $P < 0.0001$ between SSc and other groups, respectively) (Figure 5 B). Similar results were obtained repeating the assay with peptide 1, whereas peptide 3 was less efficient, inhibiting binding of 50% (17/34) of SSc sera, 8.8% (3/34) of HC and none (0/18) of PRP sera (data available upon request). To confirm that inhibition was due to specific binding of peptide 2 to serum IgG , the assay was repeated using IgG purified from 8/24 positive SSc sera and from the 4 positive HC sera. While binding of SSc IgG was inhibited by peptide 2, HC IgG were no longer inhibited (data available upon request), suggesting the presence of serum components mediating binding of HC sera to peptide 2.

C. Competitive ELISA between sera and VH_{PAM}-Vκ16F4:

to confirm that SSc sera contain autoantibodies similar to VH_{PAM}-Vκ16F4, the sera tested in *B.* were incubated onto immobilized PDGFRα-His before adding biotinylated VH_{PAM}-Vκ16F4. The 24/34 SSc sera previously inhibited by peptide 2 significantly diminished VH_{PAM}-Vκ16F4 binding to PDGFRα. Only 2/34 (5.9%) HC and 2/18 (11.1%) PRP sera inhibited binding (Figure 5 C). Spearman's rank correlation indicated that in the SSc group ($P < 0.0001$, r = 0.678), but not in the HC ($P = 0.403$, r = -0.147) and PRP ($P = 0.668$, r = -0.108) groups, the results of assays *B.* and *C.* were statistically associated.

Finally, direct and competitive ELISA were performed with sera from 29 consecutive SLE patients (SLEDAI range: 2-20). PDGFRα binding distribution of SLE sera was comparable to those of HC

sera in assay *A.* and was not influenced by disease activity index or peptide 2 competition (Figure 5 D).

Comparison between ELISA and ROS assays in SSc patients and healthy controls

IgG purified from 24/34 SSc sera analyzed by direct and competitive ELISA (Figure 5 A, B) and from four sera negative in direct ELISA (Figure 5A) were tested by ROS assay (3) (Table 1A). All sera positive by direct ELISA, including 16 samples positive and eight negative by competitive ELISA, contained ROS-inducing IgG, except serum #435, which was negative in competitive ELISA. Conversely, the four sera (#417, #433, #421, #424) negative in direct ELISA did not contain ROS-inducing IgG. The ROS-inducing activity of the seven samples negative in competitive ELISA (*i.e.,* not containing antibodies with the same specificity of VH_{PAM}-Vκ16F4) was abolished by the PDGFR tyrosine kinase inhibitor AG1296, further suggesting that VH_{PAM}-Vκ16F4-like IgG is not the only agonistic anti-PDGFRα autoantibody species. HC IgG positive in direct ELISA did not induce ROS, except samples #31S and #356 which induced ROS through a PDGFR-independent mechanism, since ROS were unaffected by AG1296 (Table 1B).

Discussion

Human PDGFRα has been implicated in a variety of diseases, including cancer, atherosclerosis and fibrosis (31-33); however, the PDGFRα domains critical for disease pathogenesis are not completely defined. *In vitro* mutagenesis (26) and crystallographic (34) studies indicated that the amino acid residues involved in receptor binding by PDGF are located in the Ig-like extracellular domains 1, 2 and 3. The rHumaab generated from PDGFRα-specific memory B cells of one SSc patient extend this information by identifying regions of the receptor transducing signals to NADPH oxidase (35, 36) and to collagen genes (37). These regions can largely overlap the canonical PDGF binding site (epitope of VH_{PAM}-Vκ16F4), or be distinct from it (epitope of VH_{PAM}-Vλ16F4). We suggest that these different PDGFRα motifs, when stimulated, modulate local or/and long distance

propagation of signals of the activated receptor that selectively govern complex phenotypes such as fibrosis and oxidative stress (38). This study reconciles the controversial results concerning the existence of stimulatory anti-PDGFR antibodies in SSc (4, 5), demonstrating that: i. stimulatory and non-stimulatory anti-PDGFRα autoantibodies may coexist in the same SSc patient; ii. stimulatory anti-PDGFRα autoantibodies recognize specific conformational epitopes, which must be preserved in binding assays to discriminate agonistic from total antibodies, and can be mimicked by specific peptides; iii. stimulatory anti-PDGFRα autoantibodies specific for these conformational epitopes are enriched in the serum of SSc patients. Moreover, the comparison between the ROS bioassay previously employed (3) and the peptide-based competitive ELISA described herein, using IgG purified from the same SSc and HC sera, although performed with a limited number of samples, indicated a remarkable concordance. The discordant results, *i.e.* the seven SSc samples testing negative by competitive ELISA but positive by ROS bioassay, can also be meaningfully interpreted. Indeed, these samples became unable to induce ROS in the presence of a specific PDGFR tyrosine kinase inhibitor, which demonstrates that they contain agonistic PDGFRα-specific antibodies. These antibodies differ from VH_{PAM}-Vκ16F4 since they are not inhibited by peptide 2. It is tempting to speculate that they are similar to VH_{PAM}-Vλ16F4, the other agonistic antibody cloned from the SSc patient. The presence of different agonistic PDGFRα-specific antibodies, binding distinct epitopes, may account for the lower sensitivity of the competitive ELISA based on one epitope, compared to the ROS bioassay. Notably, the combined analysis of antibody binding and ROS production highlighted the existence of a subgroup of SSc patients without stimulatory anti-PDGFRα IgG. This group was not found in the previous small SSc cohort in which only ROS activity was measured (3). Non-stimulatory anti-PDGFRα antibodies have been identified by others in SSc and SLE patients and in HC (5, 6). Our data confirm these findings, and indicate that complete discrimination between nonagonistic and agonistic autoantibodies can be achieved only by combination of epitope-based binding assays and functional assays. Of note, IgG purified from

the two HC and PRP sera inhibiting binding of biotinylated VH_{PAM}-Vκ16F4 to PDGFRα did not induce ROS (data available upon request). The assessment of the diagnostic relevance of stimulatory anti-PDGFRα antibodies, *i.e.* their efficacy in discriminating patients affected by early stage SSc from patients affected by related conditions such as PRP, will require the prospective screening of large cohorts of patients suspected for SSc (39) by optimized peptide-based assays. Moreover, the longitudinal analysis of agonistic anti-PDGFRα antibodies during disease progression will indicate their potential usefulness as SSc biomarker (40). Notably, the 24 SSc patients testing positive at both competitive ELISAs had a more severe disease phenotype than the 10 negative ones, but this observation must be confirmed in larger cohorts of patients. Finally, recent reports suggest that PDGFR inhibition may be a therapeutic option for SSc and other fibrotic conditions (41). Abrogation of VH_{PAM}-Vk16F4-induced collagen gene overexpression by selective mutation of the minimal epitope motif and inhibition of SSc IgG-induced ROS production and collagen overexpression by use of peptides mimicking the epitope itself, further corroborate this possibility, hinting to promising new therapeutic strategies against SSc and other pathologic conditions characterized by oxidative stress, fibrosis and abnormal PDGFR signaling.

Acknowledgments

We thank Dennis Burton, Ann Hessel and Michael Zwick (Department of Immunology, The Scripps Research Institute, La Jolla, CA, USA) for providing the pDR12 vector; Stefania Mancini (Dipartimento di Scienze Cliniche e Molecolari, Università Politecnica delle Marche, Ancona, Italy) for help with the FACS analysis; Hetian Lei (The Schepens Eye Research Institute, Harvard Medical School, Boston, MA, USA) for providing the retroviral vector p*LHDCX*^{2} containing the full-length human PDGFRα cDNA; Patrizia Bagnarelli, Stefano Menzo and Pietro Emanuele Varaldo (Dipartimento di Scienze Biomediche e Sanità Pubblica, Università Politecnica delle Marche, Ancona, Italy) for providing the BSL3 facility; Milena Maule and Erika Ortolan

(Dipartimento di Scienze Mediche, Università di Torino, Italy) for help with the statistical analysis of ELISA data; and Eline Luning Prak (Human Immunology Core Laboratory, Perelman School of Medicine, University of Pennsylvania, Philadelphia, PA, USA) for critical reading of the manuscript.

This work was supported by a Young Investigator Award from Gruppo Italiano Lotta alla Sclerodermia (GILS) to G.M., grants from Ministero Italiano per l'Università e la Ricerca Scientifica to A.G., E.V.A. and A.F., grant IG111364 from the Italian Association for Cancer Research (AIRC) to E.V.A., grants from Fondazione Cariverona and Fondazione Italiana Ricerca Artrite (FIRA) to A.G., and from Fondazione di Medicina Molecolare e Terapia Cellulare, Università Politecnica delle Marche, Ancona, Italy. G.N. is a fellow of the Fondazione Umberto Veronesi.

Author contributions

All authors were involved in drafting the article or revising it critically for important intellectual content, and all authors approved the final version to be published. Drs. Moroncini and Gabrielli had full access to all of the data in the study and take responsibility for the integrity of the data and the accuracy of the data analysis.

Study conception and design. Moroncini, Funaro, Gabrielli.

Acquisition of data. Grieco, Nacci, Paolini, Tonnini, Pozniak, Cuccioloni, Mozzicafreddo, Svegliati, Kazlauskas.

Analysis and interpretation of data. Moroncini, Angeletti, Avvedimento, Funaro, Gabrielli.

References

1. Gabrielli A, Avvedimento EV, Krieg T. Scleroderma. N Engl J Med 2009;360(19):1989-2003.

2. Varga J, Abraham D. Systemic sclerosis: a prototypic multisystem fibrotic disorder. J Clin Invest 2007;117(3):557-67.

3. Baroni SS, Santillo M, Bevilacqua F, Luchetti M, Spadoni T, Mancini M, et al. Stimulatory autoantibodies to the PDGF receptor in systemic sclerosis. N Engl J Med 2006;354(25):2667-76.

4. Classen JF, Henrohn D, Rorsman F, Lennartsson J, Lauwerys BR, Wikstrom G, et al. Lack of evidence of stimulatory autoantibodies to platelet-derived growth factor receptor in patients with systemic sclerosis. Arthritis Rheum 2009;60(4):1137-44.

5. Loizos N, Lariccia L, Weiner J, Griffith H, Boin F, Hummers L, et al. Lack of detection of agonist activity by antibodies to platelet-derived growth factor receptor alpha in a subset of normal and systemic sclerosis patient sera. Arthritis Rheum 2009;60(4):1145-51.

6. Kurasawa K, Arai S, Owada T, Maezawa R, Kumano K, Fukuda T. Autoantibodies against platelet-derived growth factor receptor alpha in patients with systemic lupus erythematosus. Mod Rheumatol 2010;20(5):458-65.

7. Dragun D, Distler JH, Riemekasten G, Distler O. Stimulatory autoantibodies to platelet-derived growth factor receptors in systemic sclerosis: what functional autoimmunity could learn from receptor biology. Arthritis Rheum 2009;60(4):907-11.

8. LeRoy EC, Black C, Fleischmajer R, Jablonska S, Krieg T, Medsger TA, Jr., et al. Scleroderma (systemic sclerosis): classification, subsets and pathogenesis. J Rheumatol 1988;15(2):202-5.

9. Traggiai E, Becker S, Subbarao K, Kolesnikova L, Uematsu Y, Gismondo MR, et al. An efficient method to make human monoclonal antibodies from memory B cells: potent neutralization of SARS coronavirus. Nat Med 2004;10(8):871-5.

10. Funaro A, Gribaudo G, Luganini A, Ortolan E, Lo Buono N, Vicenzi E, et al. Generation of potent neutralizing human monoclonal antibodies against cytomegalovirus infection from immune B cells. BMC Biotechnol 2008;8:85.

11. Shannon-Lowe C, Baldwin G, Feederle R, Bell A, Rickinson A, Delecluse HJ. Epstein-Barr virus-induced B-cell transformation: quantitating events from virus binding to cell outgrowth. J Gen Virol 2005;86(Pt 11):3009-19.

12. Andrews A, Balciunaite E, Leong FL, Tallquist M, Soriano P, Refojo M, et al. Platelet-derived growth factor plays a key role in proliferative vitreoretinopathy. Invest Ophthalmol Vis Sci 1999;40(11):2683-9.

13. Welschof M, Terness P, Kolbinger F, Zewe M, Dubel S, Dorsam H, et al. Amino acid sequence based PCR primers for amplification of rearranged human heavy and light chain immunoglobulin variable region genes. J Immunol Methods 1995;179(2):203-14.

14. Burton DR, Pyati J, Koduri R, Sharp SJ, Thornton GB, Parren PW, et al. Efficient neutralization of primary isolates of HIV-1 by a recombinant human monoclonal antibody. Science 1994;266(5187):1024-7.

15. Moroncini G, Kanu N, Solforosi L, Abalos G, Telling GC, Head M, et al. Motif-grafted antibodies containing the replicative interface of cellular PrP are specific for PrPSc. Proc Natl Acad Sci U S A 2004;101(28):10404-9.

16. Svegliati S, Cancello R, Sambo P, Luchetti M, Paroncini P, Orlandini G, et al. Platelet-derived growth factor and reactive oxygen species (ROS) regulate Ras protein levels in primary human fibroblasts via ERK1/2. Amplification of ROS and Ras in systemic sclerosis fibroblasts. J Biol Chem 2005;280(43):36474-82.

17. Schwede T, Kopp J, Guex N, Peitsch MC. SWISS-MODEL: An automated protein homology-modeling server. Nucleic Acids Res 2003;31(13):3381-5.

18. Oefner C, D'Arcy A, Winkler FK, Eggimann B, Hosang M. Crystal structure of human platelet-derived growth factor BB. Embo J 1992;11(11):3921-6.

19. Comeau SR, Gatchell DW, Vajda S, Camacho CJ. ClusPro: an automated docking and discrimination method for the prediction of protein complexes. Bioinformatics 2004;20(1):45-50.

20. Timmerman P, Puijk WC, Meloen RH. Functional reconstruction and synthetic mimicry of a conformational epitope using CLIPS technology. J Mol Recognit 2007;20(5):283-99.

21. Timmerman P, Meloen RH, Puijk WC, Boshuizen RS, van Dijken P, Slootstra JW, et al. Functional reconstruction of structurally complex epitopes using CLIPS™ Technology. The Open Vaccine Journal 2009;2:56-67.

22. Cui J, Lei H, Samad A, Basavanthappa S, Maberley D, Matsubara J, et al. PDGF receptors are activated in human epiretinal membranes. Exp Eye Res 2009;88(3):438-44.

23. Miller AD, Buttimore C. Redesign of retrovirus packaging cell lines to avoid recombination leading to helper virus production. Mol Cell Biol 1986;6(8):2895-902.

24. Lei H, Velez G, Hovland P, Hirose T, Gilbertson D, Kazlauskas A. Growth factors outside the PDGF family drive experimental PVR. Invest Ophthalmol Vis Sci 2009;50(7):3394-403.

25. Cuccioloni M, Moroncini G, Mozzicafreddo M, Pozniak KN, Nacci G, Grieco A, et al. Biosensor-based Binding Assay for Platelet-Derived Growth Factor Receptor-alpha Autoantibodies in Human Serum. J Anal Bioanal Tech S 2013;7:38-72.

26. Yu JC, Mahadevan D, LaRochelle WJ, Pierce JH, Heidaran MA. Structural coincidence of alpha PDGFR epitopes binding to platelet-derived growth factor-AA and a potent neutralizing monoclonal antibody. J Biol Chem 1994;269(14):10668-74.

27. Lokker NA, O'Hare JP, Barsoumian A, Tomlinson JE, Ramakrishnan V, Fretto LJ, et al. Functional importance of platelet-derived growth factor (PDGF) receptor extracellular immunoglobulin-like domains. Identification of PDGF binding site and neutralizing monoclonal antibodies. J Biol Chem 1997;272(52):33037-44.

28. Corti D, Voss J, Gamblin SJ, Codoni G, Macagno A, Jarrossay D, et al. A neutralizing antibody selected from plasma cells that binds to group 1 and group 2 influenza A hemagglutinins. Science;333(6044):850-6.

29. Tauriello DV, Jordens I, Kirchner K, Slootstra JW, Kruitwagen T, Bouwman BA, et al. Wnt/beta-catenin signaling requires interaction of the Dishevelled DEP domain and C terminus with a discontinuous motif in Frizzled. Proc Natl Acad Sci U S A;109(14):E812-20.

30. Goundry B, Bell L, Langtree M, Moorthy A. Diagnosis and management of Raynaud's phenomenon. Bmj 2012;344:e289.

31. Andrae J, Gallini R, Betsholtz C. Role of platelet-derived growth factors in physiology and medicine. Genes Dev 2008;22(10):1276-312.

32. Ostman A. PDGF receptors-mediators of autocrine tumor growth and regulators of tumor vasculature and stroma. Cytokine Growth Factor Rev 2004;15(4):275-86.

33. Olson LE, Soriano P. Increased PDGFRalpha activation disrupts connective tissue development and drives systemic fibrosis. Dev Cell 2009;16(2):303-13.

34. Shim AH, Liu H, Focia PJ, Chen X, Lin PC, He X. Structures of a platelet-derived growth factor/propeptide complex and a platelet-derived growth factor/receptor complex. Proc Natl Acad Sci U S A 2010;107(25):11307-12.

35. Heldin CH, Westermark B. Mechanism of action and in vivo role of platelet-derived growth factor. Physiol Rev 1999;79(4):1283-316.

36. Schlessinger J. Cell signaling by receptor tyrosine kinases. Cell 2000;103(2):211-25.

37. Smaldone S, Olivieri J, Gusella GL, Moroncini G, Gabrielli A, Ramirez F. Ha-Ras stabilization mediates pro-fibrotic signals in dermal fibroblasts. Fibrogenesis Tissue Repair 2011;4(1):8.

38. Gabrielli A, Svegliati S, Moroncini G, Amico D. New insights into the role of oxidative stress in scleroderma fibrosis. Open Rheumatol J 2012;6:87-95.

39. Avouac J, Fransen J, Walker UA, Riccieri V, Smith V, Muller C, et al. Preliminary criteria for the very early diagnosis of systemic sclerosis: results of a Delphi Consensus Study from EULAR Scleroderma Trials and Research Group. Ann Rheum Dis 2011;70(3):476-81.

40. Koenig M, Dieude M, Senecal JL. Predictive value of antinuclear autoantibodies: the lessons of the systemic sclerosis autoantibodies. Autoimmun Rev 2008;7(8):588-93.

41. Bournia VK, Evangelou K, Sfikakis PP. Therapeutic inhibition of tyrosine kinases in systemic sclerosis: a review of published experience on the first 108 patients treated with imatinib. Semin Arthritis Rheum 2012;42(4):377-90.

Figure legends

Figure 1.

Characterization of PAM 13B8, PAM 16F4, PAM 17H8 IgG. **A**, Flow cytometric analysis of IgG binding (white profile) to Fα or F-/- cells. Shaded profile is background fluorescence. ROS production was measured in Fα cells by DCFH-DA fluorescence and expressed as relative fluorescence units (RFU). Results represent the mean ± SEM of three experiments (*$P < 0.05$). **B**, Subgroup specificity of PCR amplified IgG cDNA fragments identified in PAM 13B8, 16F4 and 17H8 cells. VH or VL chain sequences with the same color encode for the same transcripts. The VH chain (blue) shared by PAM 13B8, 16F4 and 17H8 cell lines, was designated VH_{PAM}. The VL sequences were classified according to the κ or λ subgroups and the PAM cell line in which they were first identified. **C**, PDGFRα was immunoprecipitated (IP) from human fibroblasts with the four rHumaab and visualized by western blotting (WB) using an anti-PDGFRα antibody. Anti-PDGFRα mab1264 was used as control. **D**, Levels of ROS, p-AKT, p-ERK1/2 and Ha-Ras and collagen induction in human fibroblasts treated with rHumaab or PDGF-BB. Histograms represent the mean RFU or collagen expression fold increase values ± SEM of three experiments performed in duplicate (*$P < 0.05$, **$P < 0.01$).

Figure 2.

Epitope mapping of human PDGFRα. **A**-**D** (left panels), Molecular docking models of monomeric PDGF-BB or the indicated rHumaab Fab fragments bound to the extracellular region of monomeric PDGFRα, encompassing the five Ig-like domains, labeled I-V from the N- to the C-terminus. Below each model, the amino acid sequence of the first three N-terminal extracellular domains of PDGFRα is shown. Along this sequence, the amino acids composing the predicted PDGF-BB and rHumaab binding sites are highlighted by colors. The binding sites identified in the PDGFRα peptide library are underlined. **B**-**D** (right panels), Binding curves [measured in arc/seconds (arcsec)

over time] of the specific rHumaab to PDGFRα-His immobilized onto the biosensor chip, alone (no hash mark) or after saturation of PDGFRα-His with PDGF-BB ($^{\#}$),VH_{PAM}-Vκ13B8 ($^{\#\#}$) or VH_{PAM}-Vλ16F4 ($^{\#\#\#}$).

Figure 3.

Specific PDGFRα peptides interfere with binding and functions of the agonistic VH_{PAM}-Vκ16F4 rHumaab and of IgG from SSc sera. **A**, Binding of VH_{PAM}-Vκ16F4, VH_{PAM}-Vλ16F4 and VH_{PAM}-Vκ13B8 to immobilized peptides 1, 2, 3. **B**, Binding of VH_{PAM}-Vκ16F4 or PDGF-BB to immobilized PDGFRα-His with or without pre-incubation with peptides (molar ratio peptide: PDGFRα = 50:1) (***$P < 0.001$). **C**, Collagen induction by VH_{PAM}-Vκ16F4 with or without pre-incubation with peptides (molar ratio peptide:rHumaab = 100:1). Asterisks indicate the statistical significance of inhibition of Col1A1 and Col1A2 gene induction in human fibroblasts exposed to VH_{PAM}-Vκ16F4 pre-incubated with peptides (*$P < 0.05$, **$P < 0.01$). **D**, Equal amounts of pooled IgG purified from sera of six SSc patients or six HC subjects were used to induce collagen gene expression or ROS production with or without pre-incubation with peptides. Peptide 2 inhibits SSc IgG-induced Col1A1 and peptide 1 and 2 inhibit ROS production(*$P < 0.05$). Col1A1 mRNA expression or ROS production were increased by SSc IgG ($P < 0.05$), TGFβ ($P < 0.0001$) or PDGF-BB ($P < 0.05$), but not by HC IgG. Histograms represent the mean ± SEM of three independent experiments performed in duplicate.

Figure 4.

Mutagenesis of the discontinuous epitope of the agonistic VH_{PAM}-Vκ16F4 rHumaab. **A**, Visualization of the PDGFRα conformational epitope of VH_{PAM}-Vκ16F4. Epitope surface amino acid residues composing the VH_{PAM}-Vκ16F4 binding site predicted by molecular docking are highlighted and rendered as light blue sticks. The corresponding translucent Van der Waals surface

is superimposed to depict the VH_{PAM}-Vκ16F4 binding pocket. Secondary structures of PDGFRα are displayed using the ribbon representation. The different sites of alanine mutations (Ala-scans) are emphasized by dotted squares. **B**, FACS analysis of cell surface PDGFRα expressed by Fα and Ala-scan-expressing F-/- cells stained with VH_{PAM}-Vκ16F4 and mab 1264, binding to a different epitope of PDGFRα extracellular domain. F-/- cells were used as negative control. **C**, Collagen gene induction measured by real-time qPCR. Mouse type I collagen mRNA levels in Fα, F-/- and Ala-scan-expressing cells exposed to VH_{PAM}-Vκ16F4, normalized to the mean values of endogenous Cyclophilin A. Histograms represent the mean relative expression fold increase ± SEM of three experiments performed in duplicate, calculated by the 2-ΔΔCt method. (**P* < 0.05).

Figure 5.

Detection of serum anti-PDGFRα autoantibodies. **A**, Direct ELISA of sera from SSc, HC and PRP subjects. The horizontal line indicates the median (****P* < 0.0001). O.D. = 0.129 is the optimal cut-off for PDGFRα binding between positive and negative sera, determined by ROC curve of SSc *versus* HC [sensitivity = 94.4%, specificity = 51.5%, AUC = 0.801 with 95% CI = 0.793 to 0.854]. **B**, Peptide 2 inhibits SSc sera binding to PDGFRα. Median percentage binding inhibition of SSc sera = 36.05 *versus* 21.2 in HC sera and 3.6 in PRP sera (***P* < 0.001 between SSc and HC; ****P* < 0.0001 between SSc and PRP). Inhibition = 29.8% represents the optimal cut-off discriminating sera whose binding to PDGFRα is significantly inhibited by peptide 2, determined by ROC curve (sensitivity = 70.6%, specificity = 88.2%, AUC = 0.764 with 95% CI = 0.645 to 0.858). **C**, Binding inhibition of VH_{PAM}-Vκ16F4 to PDGFRα by sera. Median percentage of VH_{PAM}-Vκ16F4 binding inhibition by SSc sera = 30.60 *versus* 11.65 by HC and 5.45 by PRP sera (****P* < 0.0001). Inhibition = 26.1% is the optimal cut-off discriminating sera inhibiting from those weakly or not inhibiting VH_{PAM}-Vκ16F4 binding to PDGFRα, determined by ROC curve (sensitivity = 70.6;

specificity = 94.1; AUC = 0.760 with 95% CI = 0.641 to 0.856). **D**, Direct or competitive ELISA of SLE sera. Each dot corresponds to the mean O.D. of each sample, tested in triplicate.

Table 1.

Comparison between ELISA and ROS assays in SSc patients and HC subjects. Melon gel-purified IgG (200 µg/ml) from **A**, 24 SSc serum samples that had been subjected to both direct and competitive ELISA and 4 SSc serum samples testing negative to direct ELISA, and **B**, from 26 HC serum samples of which 24 positive and 2 negative in the anti-PDGFRα direct ELISA, were tested for their ability to induce ROS production in Fα cells. Red color indicates values over the cut-off and blue color indicates values under the cut-off. Binding: cut-off = 0.129 (O.D. column); % binding inhibition by peptide 2: cut-off = 29.8; ROS: cut-off = 0.4 (stimulation index, SI). SI = (S − C) ÷ (P − C), where S is the DCF fluorescence intensity of the test IgG, C is the DCF fluorescence intensity of a negative control obtained by culturing cells without IgG, and P is the DCF fluorescence intensity of a positive control obtained by incubating cells with PDGF (15 ng/ml for 15 minutes). Samples able to induce ROS were tested in the presence of PDGFRα inhibitor AG1296 (2 µM).

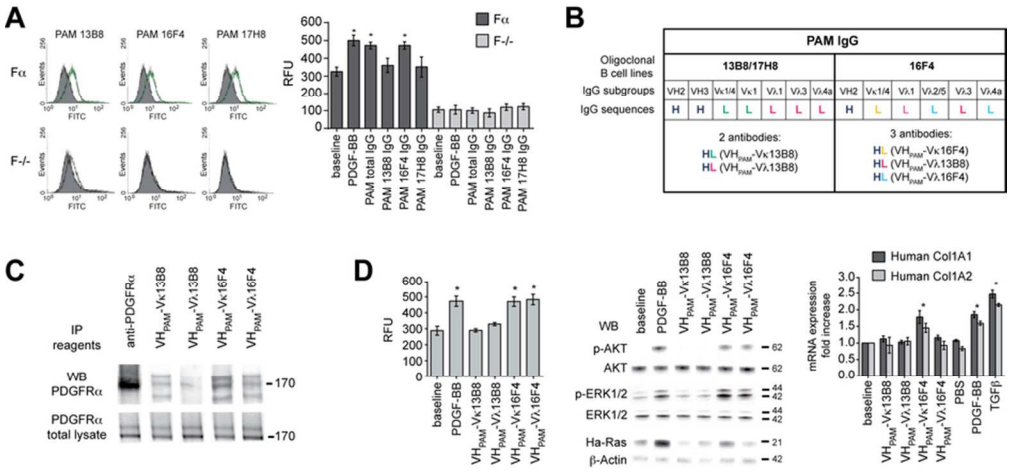

79x36mm (300 x 300 DPI)

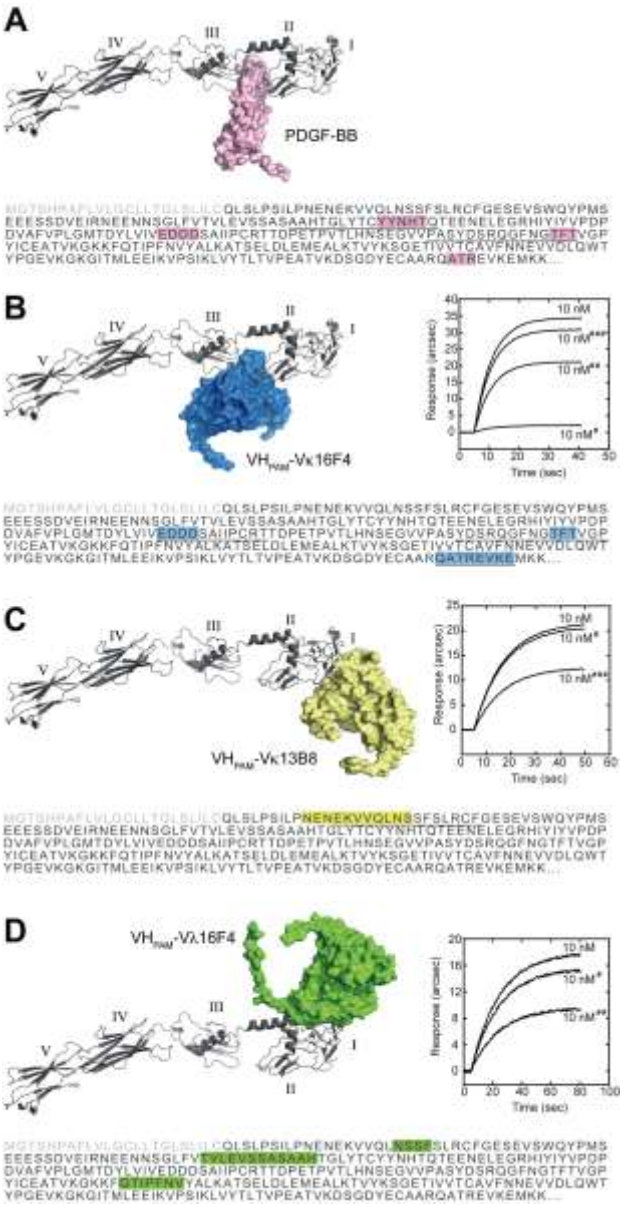

155x300mm (300 x 300 DPI)

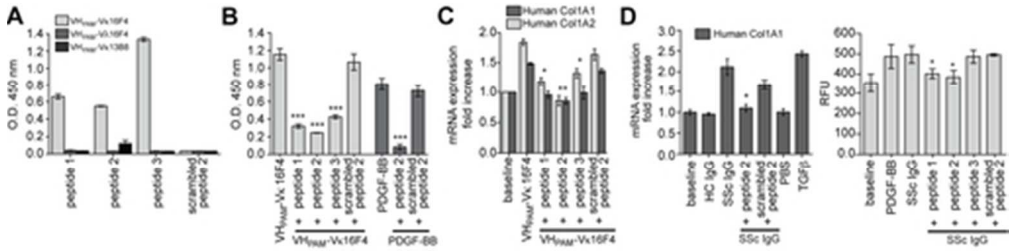

43x10mm (300 x 300 DPI)

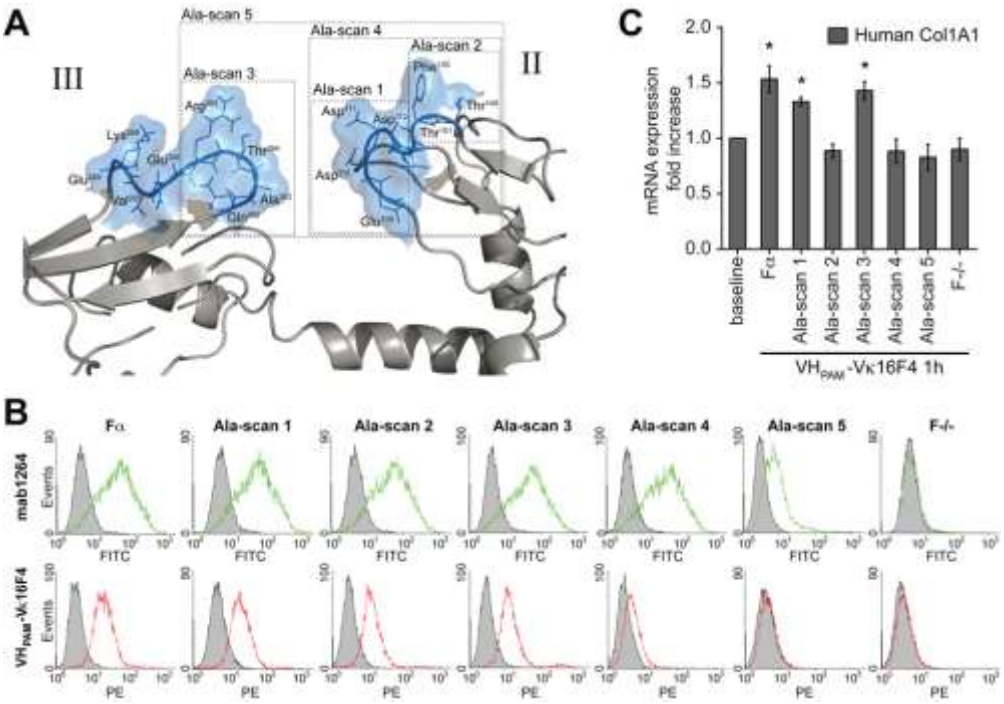

81x56mm (300 x 300 DPI)

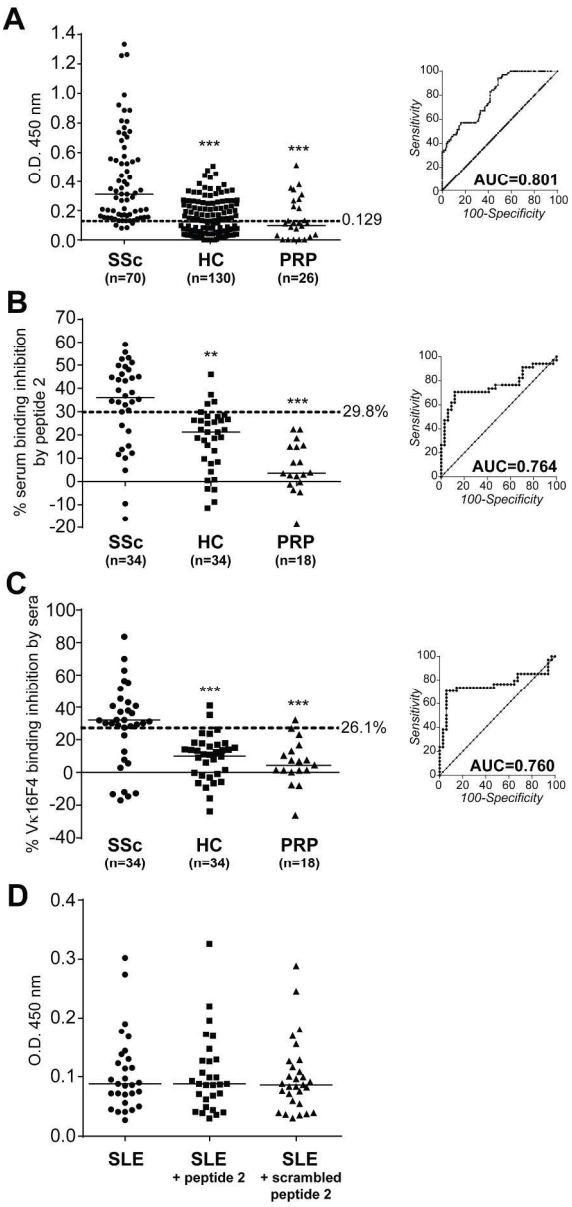

165x352mm (300 x 300 DPI)

A

SSc (n=28)				
serum sample	serum binding (O.D.)	% serum binding inhibition by peptide 2	IgG-induced ROS (S.I.)	ROS + AG1296 (S.I.)
406	0.583	51.1	1.03	
429	0.456	49.8	0.40	
422	0.382	46.1	0.73	
#SP	0.333	44.4	0.59	
413	0.281	29.9	1.15	
210	0.269	35.3	1.15	
108	0.261	49.3	0.74	
211	0.259	34.1	0.50	
427	0.229	30.6	1.13	
221	0.194	34.2	1.60	
404	0.178	34.5	0.87	
425	0.171	53.1	1.21	
410	0.165	43.2	1.42	
111	0.146	36.8	1.68	
411	0.141	39.2	1.23	
418	0.129	32.9	1.23	
416	0.179	4.8	1.51	0.17
434	0.175	10.1	1.80	0.00
114	0.169	-9.5	1.51	0.00
409	0.155	-16.2	1.31	0.10
4S	0.151	12.2	0.81	0.00
414	0.143	21.6	0.85	0.18
217	0.186	13.8	0.53	0.36
435	0.170	11.6	0.00	
417	0.114		0.11	
433	0.100		0.08	
421	0.084		0.00	
424	0.080		0.28	

B

HC (n=26)			
serum sample	binding (O.D.)	IgG-induced ROS (S.I.)	ROS + AG1296 (S.I.)
109	0.000	0.07	
376	0.091	0.15	
154	0.220	0.00	
234	0.227	0.00	
311	0.164	0.00	
316	0.210	0.00	
330	0.178	0.00	
341	0.201	0.00	
352	0.140	0.00	
384	0.129	0.00	
23S	0.266	0.00	
149	0.130	0.00	
223	0.446	0.00	
225	0.225	0.00	
230	0.266	0.04	
224	0.350	0.10	
353	0.139	0.13	
34S	0.164	0.17	
148	0.168	0.27	
32S	0.147	0.29	
333	0.266	0.30	
314	0.190	0.33	
228	0.191	0.34	
233	0.174	0.40	
31S	0.190	0.61	0.63
356	0.304	0.72	0.80